Nanoscale

Halide Exchange and Surface Modification of Metal Halide Perovskite Nanocrystals with Alkyltrichlorosilanes

Journal:	*Nanoscale*
Manuscript ID	NR-ART-06-2018-004763.R1
Article Type:	Paper
Date Submitted by the Author:	01-Aug-2018
Complete List of Authors:	Uddin, Md; University of Kentucky, Chemistry Calabro, Rosemary; University of Kentucky, Chemistry Kim, Doo Young; University of Kentucky, Department of Chemistry Graham, Kenneth; University of Kentucky, Chemistry

Nanoscale

Paper

Halide Exchange and Surface Modification of Metal Halide Perovskite Nanocrystals with Alkyltrichlorosilanes

Received 00th January 20xx,
Accepted 00th January 20xx

DOI: 10.1039/x0xx00000x
www.rsc.org/

Md Aslam Uddin, Rosemary L. Calabro, Doo-Young Kim, and Kenneth R. Graham*

Metal halide perovskite nanocrystals have recently emerged as promising materials for light emitting displays and lasing applications due to their narrow emission wavelengths, high photoluminescence quantum yields, and readily adjustable emission wavelengths. For these metal halide perovskite nanocrystals to be useful in commercial applications, their stability must be increased and the photoluminescence quantum yields of the iodide (red emitting) and chloride (blue emitting) containing derivatives must also be increased. The photoluminescence quantum yields of blue emitting $CsPbCl_3$ nanoparticles lag those of green emitting $CsPbBr_3$ nanoparticles, with maximum photoluminescence quantum yields of 1-10% previously reported for $CsPbCl_3$ as compared to 80-100% for $CsPbBr_3$. Herein, we show that alkyltrichlorosilanes (R-$SiCl_3$) can be used as Cl-sources for rapid anion exchange with host $CsPbBr_3$ nanocrystals. This anion exchange reaction is advantageous in that it can be performed at room temperature and results in highly dispersible nanoparticles coated with siloxane shells. $CsPbCl_3$ nanoparticles produced through Cl-exchange with R-$SiCl_3$ show significantly improved long-term stability and high photoluminescence quantum yields of up to 12%. These siloxane coated nanocrystals are even stable in the presence of water, whereas $CsPbCl_3$ nanoparticles synthesized through other routes rapidly degrade in the presence of water.

INTRODUCTION

Lead-based metal halide perovskites (MHPs) have the general chemical formula of $APbX_3$, where A is methylammonium, formamidinium, or Cs and X is Cl, Br, or I. Lead-based MHPs are direct bandgap semiconductors and have high photoluminescence quantum yields (PLQYs) of up to 80-100%.[1–4] The electronic and optical properties of MHPs make these materials appealing for optoelectronic devices, such as photovoltaics (PVs),[5–8] light emitting diodes (LEDs),[9–12] lasers,[13–16] and photodetectors (PDs).[17–20] While the bulk materials are garnering significantly more interest for PVs, nanoparticles are more attractive for LEDs owing to their currently higher PLQYs.

Metal halide perovskite nanocrystals (MHPNCs) can be synthesized using low-cost precursors and relatively simple synthetic procedures.[4,21] The most widely preferred method for synthesizing MHPNCs is the hot-injection method, which was first used to synthesize highly luminescent and monodisperse colloidal $CsPbX_3$ NCs with 4-15 nm edge lengths.[4] Bandgap energies and photoluminescence (PL) emission spectra of these synthesized MHPNCs are easily tunable over the entire visible spectral range of 410-700 nm with PLQYs of up to 90% *via* adjusting the halide composition or taking advantage of quantum size-effects.[4] $CsPbX_3$ NCs show narrower size distributions than many other nanoparticles, *e.g.*, $CuInS_2$, $CuInSe_2$, Cu_2ZnSnS_4, partly because of the distinct size and charge of Pb^{2+}, Cs^+, and X^- ions.[4,22–25] The varying ion size and charge helps ensure proper order and homogeneity in the distribution of ions in the formation of nanocrystals.[4] Furthermore, MHPNCs are more ionic in nature than chalcogenide containing nanocrystals, which plays a role in making MHPNCs significantly less sensitive to surface states than chalcogenide containing nanocrystals.[4,26,27]

In addition to the direct synthesis of MHPNCs with varying halide composition, these MHPNCs can readily undergo anion exchange reactions with various halide sources in solution to vary the halide composition post-synthesis. The ease of anion exchange reactions in MHPNCs is partly attributed to the dynamic surface ligand binding of oleylammonium halide and oleylammonium oleate,[28,29] the ability of MHPNCs to retain their cubic structures at 40 ℃ due to the rigid cationic sublattice,[21,30,31] and the high ionic diffusion afforded by the vacancy-assisted diffusion mechanism,[21,30,32–34] In general, all that is needed for rapid anion exchange to occur is a source of halide ions.

Common halide ion sources for anion exchange have thus far included lithium halides (LiX),[18] lead halides (PbX_2),[21,35] oleyl/alkyl-ammonium halides (O/RAmX),[21,36] alkyl-magnesium halides (Grignard reagents, RMgX),[21] and zinc halides (ZnX_2).[37] Through tuning the concentration of the halide exchange source, the PL maximum can be adjusted over the entire visible wavelength range with narrow full width at half maximum (FWHM) of 10-40 nm while

Department of Chemistry, University of Kentucky, Lexington, Kentucky 40506, USA. E-mail: Kenneth.graham@uky.edu
Electronic Supplementary Information (ESI) available: [details of any supplementary information available should be included here]. See DOI: 10.1039/x0xx00000x

maintaining PLQYs of 1-90%.[21,35–39] In addition to solution state anion exchange reactions, Guhrenz, *et al.* demonstrated that solid state anion exchange reactions between parent MHPNCs and common NaX and KX salts occur and can be used to alter the MHPNC composition and PL emission over a wide spectral range (400 nm to 700 nm).[38] In a less conventional approach, Parobek, *et al.* carried out anion exchange reactions *via* photoexcitation of $CsPbX_3$ NCs in a solution of dihalomethane in the absence of any spontaneously reacting anion precusors.[39] However, all these methods of anion exchange reactions have their disadvantages that further complicate their synthesis and/or purification. For example, the inclusion of excess ligands in solution to help dissolve the anion exchange precursor,[28,40] the need for laser irradiation,[39] or the need for post-exchange surface treatments of synthesized NCs to maintain stablity.[1,41]

A major issue that must be overcome to facilitate commercial applications for these MHPNCs is their instability to atmospheric moisture, oxygen, and light illumination.[42–46] One means of stabilizing colloidal nanoparticles is to coat them with a stable and inert ligand shell.[3,47–49] As it has been demonstrated that the most commonly used ligands with MHPNCs, namely conjugate counterparts of oleylamine and oleic acid, bind in a highly dynamic fashion, these surface ligands are one of the reasons that MHPNCs are typically unstable in solution. In addition, to keep the nanoparticles as stable as possible in solution there must be an excess of oleylamine and oleic acid present. Surface ligands that have been used in place of oleylamine and oleic acid are thiols,[41,50] thiocyanate salts,[1] trioctylphosphine oxide,[51] 2-adamantylammonium bromide,[52] and 3-(*N*,*N*-dimethyloctadecylammonio)propane sulfonate.[53] Many of these ligands lead to higher quantum yields, but few have been shown to result in colloidal nanoparticles that are stable in solution for more than a few days. Furthermore, most of these ligands were applied to $CsPbBr_3$,[1,41,48,51] $CH_3NH_3PbBr_3$,[3,47,49,52] or $CsPbI_3$ nanoparticles.[49]

Herein, we report a simple, fast, and room temperature anion exchange reaction between host $CsPbBr_3$ NCs and alkyltrichlorosilanes. It was previously demonstrated that trichlorosilanes can be used to modify the surface of planar methylammonium lead iodide films,[54] but they have not yet been applied to perovskite nanoparticles as surface modifiers and were not previously shown to result in halide exchange with the methylammonium lead iodide films investigated. In our work, dodecyltrichlorosilane (DTS) is shown to react to form a hydrophobic shell around the nanoparticles to keep them stable in solution for extended time periods, while the Cl^- is exchanged with Br^- in the $CsPbBr_3$ NCs to produce $CsPbCl_3$ NCs. In this process we suspect DTS primarily reacts with water molecules dissolved in the dispersion of NCs, while a smaller amount of DTS may also react with hydroxyl groups or water molecules on the NC surfaces, to form hydrochloric acid and dodecylsilols. These silols may then either react with undercoordinated surface lead atoms through the formation of a Pb-O bond, or react with other molecules of DTS to produce siloxane polymers and hydrochloric acid.[55] These liberated Cl^- ions participate in the anion exchange for Br^-, while oxygen atoms in the Si-O-Si groups of siloxane polymers may coordinate to the metal centers on the surface of $CsPbCl_3$ NCs. Similar to MHPNCs coated with silsesquioxanes and SiO_2,[3,49] we show that $CsPbCl_3$ NCs produced with DTS show significantly improved stability and increased PLQYs over those of $CsPbCl_3$ NCs synthesized from alternative anion exchange methods reported in the literature.

RESULTS AND DISCUSSION

The colloidal $CsPbBr_3$ NCs were synthesized by the hot-injection method described by Nedulcu *et al.* with minor changes.[21] The NCs were purified through centrifugation, with complete procedures for synthesis and purification described in the experimental section. Figure S1a shows characteristic optical absorption and PL emission spectra of purified colloidal $CsPbBr_3$ NCs. The $CsPbBr_3$ NCs show an absorption edge at 508 nm and a PL emission maximum of 512 nm with FWHM of 17.4 nm, which is comparatively narrower than the previously reported values in the literature.[28,36,51,52] This narrower FWHM of the $CsPbBr_3$ NCs indicates that the synthesized NCs are highly monodisperse.[28,51] The PLQYs of the $CsPbBr_3$ NCs range from 39 to 74% and are dependent on the specific synthesis conditions. Particularly, the PLQYs depend on the stoichiometric ratio of $PbBr_2$ and Cs_2CO_3 as well as the reaction quenching time. The same batch of purified $CsPbBr_3$ NCs with an initial PLQY of 74% was used for the anion exchange reaction data reported herein. As shown in Figure S1b and Table S1, these $CsPbBr_3$ NCs have average radiative lifetimes of 9.4±0.1 ns, which is in the typical range for colloidal $CsPbBr_3$ NCs.[1,4,56] The transmission electron microscope (TEM) images and X-ray diffraction (XRD) patterns of the as-synthesized $CsPbBr_3$ NCs shown in Figures S2 indicates that the NCs are cubic in shape with edge length and squareness of 11.30±1.70 nm and 0.90±0.12, respectively, as shown in Figure S3.[26,28,36,57] Selected area electron diffraction (SAED) patterns in Figure S4 show the single-crystalline and cubic nature of NCs with d-spacings of 0.382 and 0.276 Å for the (110) and (200) planes, which are characteristic d-spacing values of cubic $CsPbBr_3$ NCs for (110) and (200) planes, respectively.[58–60]

Host $CsPbBr_3$ NCs were directly transformed to colloidal $CsPbCl_xBr_{3-x}$ NCs upon addition of DTS to a solution of host $CsPbBr_3$ NCs, as indicated by the UV-vis absorbance (non-normalized) and photoluminescence (PL) emission spectra (normalized) presented in Figure 1 (see inset of SI Figure S6a for non-normalized PL data). The proposed mechanism for this exchange reaction is depicted in Figure S5. Figure 1a and b show that upon addition of 50 μL DTS to a 3 mL dispersion of $CsPbBr_3$ NCs in hexane (absorbance *ca.* 0.1 at 350 nm), the absorption edge and PL maximum blue shift from 508 nm to 446 nm and 512 nm to 451 nm, respectively, within 30 minutes. Figure 1c shows that as the concentration of DTS in solution increases, the rate of reaction increases and the PL maximum plateaus at shorter wavelengths. The PL emission peaks maintain narrow FWHMs of 10.5 to 14.2 nm for all DTS concentrations investigated, as evident in Figure 1d, which agrees with previously reported data for $CsPbCl_3$ and $CsPbCl_xBr_{3-x}$.[21,35,36] Upon anion exchange the PL intensity and PLQY decrease, as

evident in Figure S6, which is in agreement with the lower PLQYs previously observed for $CsPbCl_3$ relative to $CsPbBr_3$. Figure 1c and d show that the final halide composition depends on the concentration of DTS added to the solution of $CsPbBr_3$ NCs. Phenyltrichlorosilane was also investigated and found to yield similar results, which suggests that this procedure should be applicable to any trichlorosilane containing molecule.

To compare our method of synthesizing $CsPbCl_3$ NCs with other synthetic methods, we also performed the anion exchange using $PbCl_2$ as the Cl^- source. Figure 2 shows that the $CsPbCl_3$ NCs

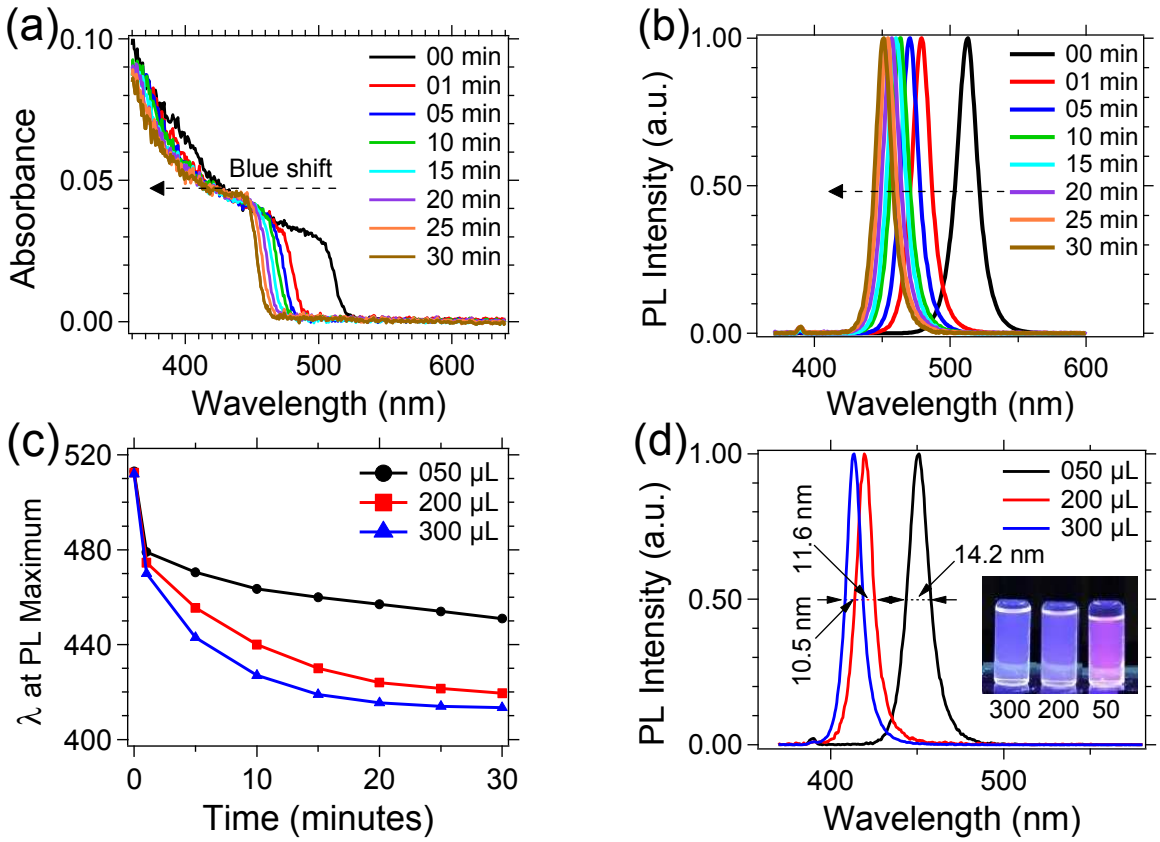

Figure 1. Time-dependent (a) UV-Vis absorbance and (b) normalized PL emission spectra of DTS assisted anion exchanged NCs during the anion exchange reaction between 3 mL $CsPbBr_3$ NC solution (absorbance *ca.* 0.1 at 350 nm) and 50 µL DTS at room temperature, (c) Time-dependent PL emission spectra showing the PL emission maximum at 5 minute intervals, and (d) PL emission spectra of DTS assisted anion exchanged NCs after 30 minutes of addition of 50, 200, and 300 µL of DTS to the 3 mL colloidal solution of host NCs at room temperature (inset: optical photographs of 50, 200, and 300 µL DTS assisted anion exchanged NCs under a 365 nm UV lamp).

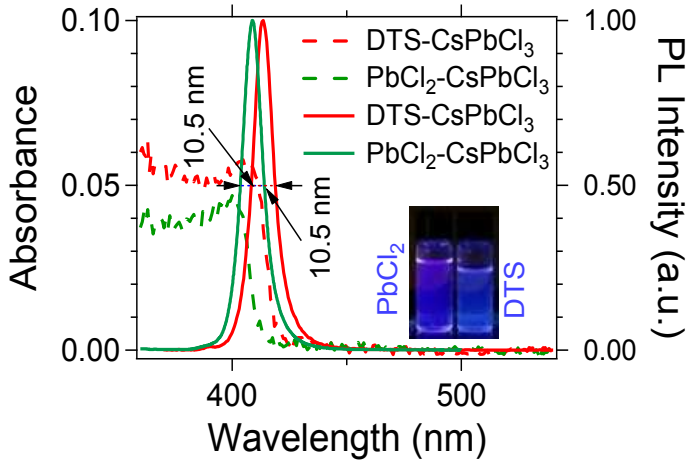

Figure 2. Optical absorption (dashed lines) and PL emission (solid lines) spectra of $CsPbCl_3$ nanocrystals produced through anion exchange with 300 µL DTS after the anion exchange reaction proceeded for 30 minutes (red) and $CsPbCl_3$ nanocrystals produced through anion exchange with $PbCl_2$ as the Cl^- source (green). Inset: optical photographs of $PbCl_2$ and 300 µL DTS assisted anion exchanged NCs under a 365 nm UV lamp.

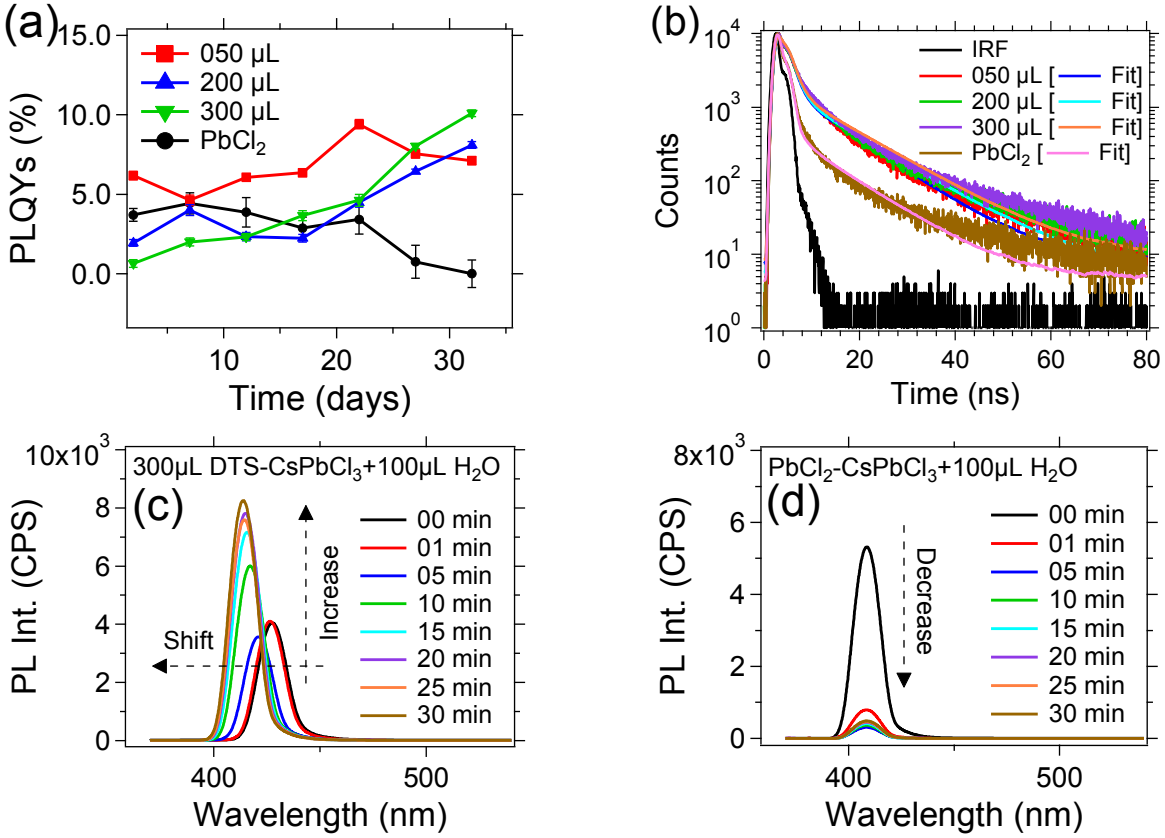

Figure 3. (a) Time-dependent PLQYs of DTS and $PbCl_2$ assisted anion exchanged NCs upon solution storage in air, (b) PL lifetime decays 2 days after anion exchange and the instrumental response function (IRF), and PL spectra changes upon adding 100 µL of water to 3 mL of (c) DTS and (d) $PbCl_2$ assisted anion exchanged NCs (absorbance values of *ca.* 0.1 at 350 nm) in hexane.

synthesized with DTS as the chloride source display similar absorption and PL spectra as those synthesized using $PbCl_2$ as the halide source, which is a commonly used Cl^- source for anion exchange.[21,36]

The PL maxima for the $CsPbCl_3$ NCs produced through Cl^- exchange with DTS and $PbCl_2$ fall at 413 and 409 nm, respectively, and display identical FWHMs of 10.5 nm. These values are comparable to the 410 nm PL maximum reported for pure $CsPbCl_3$ NCs,[4] which suggests that after 30 minutes the exchange reaction is nearly complete.

TEM images and XRD patterns were collected on both DTS and $PbCl_2$ assisted anion exchanged $CsPbBr_3$ NCs, as shown in Figures S7 and S9. The XRD spectra and lattice fringe spacings are consistent with the cubic perovskite structure ($Pm\bar{3}m$ space group) of $CsPbCl_3$ NCs,[26] as summarized in Table S2. Both DTS and $PbCl_2$ assisted anion exchanged NCs have nearly identical average crystal sizes and squareness (9.7±1.6 nm, 9.6±1.5 nm, and 0.90±0.11, respectively), as shown in Figure S8. The nearly identical sizes and shapes of both DTS and $PbCl_2$ assisted anion exchanged NCs indicates that the Cl^- source does not affect the shape and crystal structure of these NCs. Furthermore, with both Cl^- sources the NCs contract slightly in size while the shape remains nearly identical to the parent $CsPbBr_3$ NCs, which is alike to the typical halide-precursor assisted anion exchanged MHPNCs reported in the literature.[21,35,38]

Improving the stability of $CsPbBr_3$ NCs through the use of surface ligands has been a subject of recent interest;[61–63] however, $CsPbCl_3$ NCs have received much less attention in this regard. With using DTS for the Cl source, we expected that a siloxane coating would stabilize the nanoparticle. Indeed, DTS assisted anion exchanged NCs show large enhancements in stability and dispersibility over $PbCl_2$ exchanged NCs. Figure 3a shows that the PLQYs of DTS exchanged NCs increase from starting values of 1-6% to final values of 7-10% (record 12% for a different experimental run) over a period of 1 month with storage in capped vials in ambient atmosphere. By contrast, the PLQYs of $PbCl_2$ assisted anion exchanged NCs decrease to 0% over this same time frame. In addition, DTS assisted anion exchanged NCs show suppressed photobleaching compared to the $PbCl_2$ assisted anion exchanged NCs, as shown in Figure S6d. In addition, we did not observe any aggregation of DTS assisted anion exchanged NCs after one month of storage in ambient air. The stability of solid films of DTS exchanged NCs on a glass substrate were also investigated, as shown in Figure S11. We observed similar results as for the solution measurements, i.e., the PL intensity of the DTS exchanged NC films increased up to 41% after storage in air for 6 days.

We further investigated the PL properties through measuring the PL lifetimes at varying times after anion exchange, as shown in Figure 3b and SI Figure S10 and SI Table S1. The PL lifetime decays

of DTS and $PbCl_2$ assisted anion exchanged NCs are best fit with bi-exponential decays, and the average lifetimes of the NCs are within the range of previously reported values.[1,4,64,65] Two different decay pathways in the PL lifetime decays likely arise from states within the bandgap, which may arise from surface states and/or structural distortions.[1,4,31,64–67] We find that the PL lifetimes of the $CsPbCl_xBr_{3-x}$ NCs produced from DTS as the Cl^- source are 2 to 2.5 times longer than those with $PbCl_2$ as the Cl^- source at 2 and 7 days after synthesis, with values of *ca.*2 ns for $PbCl_2$ and *ca.* 5 ns for DTS. We hypothesize that this longer lifetime for the DTS assisted anion exchanged NCs arises from coordination of oxygen from the O-Si groups to undercoordinated surface Pb atoms. After 32 days, the PLQY of the $CsPbCl_3$ NCs produced from $PbCl_2$ has decreased to *ca.* 0.1%, and correspondingly the PL lifetime has decreased to only 0.24 ns. By contrast, after 32 days the PLQYs of the DTS exchanged NCs either remain similar to their values on day 7 (with 50 and 200 µL DTS) or show further increased lifetimes of 9.2 ns (with 300 µL DTS). These PL lifetimes further support that DTS significantly improves NC stability.

To further investigate the stability of the nanoparticles in the presence of water, 100 µL of deionized H_2O was directly added to 3 mL of a colloidal solution of DTS exchanged NCs 20 minutes after initial DTS addition (absorbance values of *ca.* 0.1 at 350 nm). As is evident in Figure 3c and d, the addition of water causes the PL intensity of the NCs with DTS to increase by a factor of more than two over 30 minutes; whereas, the PL intensity of the NCs with $PbCl_2$ decreases by 90% over 30 minutes. The hypsochromic PL shift for the DTS exchanged NCs is suspected to result from the additional HCl generated upon water addition, i.e., the unreacted DTS molecules react with water following the mechanism in SI Figure S5a. The higher Cl^- concentration in solution results in further halide exchange to shift the equilibria closer to pure $CsPbCl_3$ NCs. The enhanced PL intensity may be attributed to the increased amount of siloxane in solution that is available to coordinate and passivate the NC surface; or, this PL increase may result from the increased concentration of Cl^- in solution, which may help to passivate defect states on the NC surfaces (e.g., undercoordinated Pb). Longer term stability measurements, as displayed in SI Figure S11 for a separate batch of DTS exchanged NCs, show that the PL emission intensity reaches a maximum 1 day after water addition and decreases from that maximum by less than 20% after 6 days.

Fourier transform infrared absorbance (FTIR) and Raman scattering were used to further investigate the reactions of DTS and $CsPbBr_3$ NCs. Figure 4 shows the FTIR spectra of the NCs, associated organic molecules, and their conjugate counterparts (complete FTIR spectra are shown in the Figure S12a). The main observations from this data are that the DTS that remains in the NC solution following purification is completely converted to siloxane, the Si-O-Si groups appear to coordinate to the NC surface, and DTS displaces the oleylamine/oleylammonium ligands from the NC surface. In DTS assisted anion exchanged NCs, we observe the disappearance of the Si-Cl bands at 562 and 585 cm^{-1} present in pure DTS and an increase in the Si-O-Si anti-symmetric stretching modes at ~970-1200 cm^{-1}.[3,68,69] The absence of the Si-OH peak at 924 cm^{-1} in the dispersion of $CsPbCl_3$ NCs supports that the DTS molecules form siloxane polymers or Si-O-Pb bonds, as opposed to silols.[3,70] The symmetric stretching mode of Si-O-Si groups in DTS assisted anion exchanged NCs appears at 788 cm^{-1}, which is shifted from the sharp band at 765 cm^{-1} of Si-O-Si groups in the siloxane polymers formed from

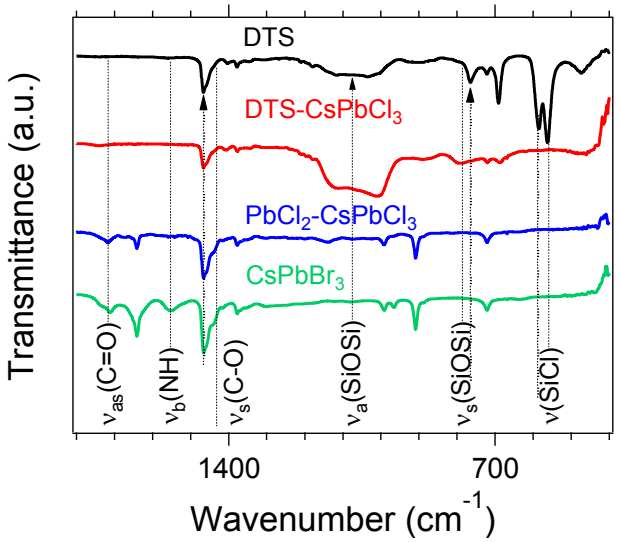

Figure 4. FTIR spectra of pure DTS, DTS assisted anion exchanged NCs, $PbCl_2$ assisted anion exchanged NCs, and host NCs.

pure DTS upon air exposure.[3,69] This peak shift may potentially arise from the Si-O-Si groups coordinating to the Pb centers on the NC surfaces. Another peak appears at 1054 cm^{-1} in DTS assisted anion exchanged NCs, shown in SI Figure S12a, which we suspect is due to Si-O-Si coordinated to Pb on the NC surface.

The displacement of oleylamine/oleylammonium by DTS is evident by the absence of the N-H stretching mode and bending modes at ~3301 and 1552 cm^{-1}, respectively, which are both observed in the FTIR spectra of the host NCs and $PbCl_2$ assisted anion exchanged NCs.[57] The displacement of oleylamine/oleylammonium by DTS is further supported by the absence of the N-H bending mode peaks at 1644 cm^{-1} in the Raman spectra of DTS exchanged NCs, as shown in Figure S13.[71] The Raman and FTIR data show that a fraction of carboxylate ions remain bound to the NC surface following DTS assisted anion exchange, which can be attributed to their stronger binding affinity as compared to amines.[28,29] This claim is supported by the shoulder observed at ~1435 cm^{-1}, which is attributed to the C-O bond of carboxylate ions, in the IR spectra of host NCs, $PbCl_2$ assisted anion exchanged NCs, and DTS assisted anion exchanged NCs.[50,72] The Raman spectra also show a shoulder at 1420 cm^{-1} due to the C-O bond of carboxylate ions in the colloidal solution of DTS assisted anion exchanged NCs.[73] In the FTIR spectra of DTS assisted anion exchanged NCs, stretching peaks from =C-H at 3077 cm^{-1} and C=O at ~1710 cm^{-1} from ODE and carboxylic acid, respectively are absent. The absence of these two peaks from ODE and OA indicates removal of pure ODE and OA from the colloidal NCs during purification.

CONCLUSIONS

Perovskite NCs are attractive for light emitting applications, and this work provides an important step in developing methods for synthesizing highly luminescent and stable blue-emitting perovskite NCs. The alkyltrichlorosilane assisted anion exchange reactions demonstrated have several advantages compared to methods reported in the literature, including shorter reaction times, room temperature synthesis, no need for excess ligands or any exchange precursor work up, and the ability of DTS to act as both an anion source and surface modifier. The siloxanes also passivate the NC surfaces and stabilize the NCs, resulting in increased PLQYs and high stability upon both storage in air and exposure to water. This discovery paves the way towards using a number of trichlorosilane derivatives as surface modifiers to further control and enhance the optical properties, electronic properties, and stability of chloride containing perovskite NCs.

EXPERIMENTAL SECTION

Materials and Chemicals

Cs_2CO_3 (99.9%, metal basis, Alfa Aesar), octadecene (ODE, tech. 90%, ACROS Organics), oleic acid (OA, tech.90%, Alfa Aesar), oleylamine (OAm, >40%, TCI), $PbCl_2$ (puratronic 99.99%, metal basis, Alfa Aesar), $PbBr_2$ (puratronic 99.99%, metal basis, Alfa Aesar), dodecyltrichlorosilane (DTS, >97.0%, TCI), and hexane (ACS grade, BDH) were purchased and used as received.

Preparation of Cs-Oleate

0.1015 g of Cs_2CO_3, 5.0 mL of octadecene (ODE), and 0.39 mL of oleic acid (OA) were added to a 2-necked 50 mL reaction flask. The flask was heated at 120 °C for 1 hour under vacuum while stirring the solution mixture at 400 rpm. For dissolving Cs_2CO_3 completely and forming Cs-oleate, the temperature of solution mixture in the flask was raised to 150 °C under a N_2 environment while stirring the solution mixture at 400 rpm.

Synthesis and Purification of $CsPbBr_3$ Nanocrystals

68.6 mg of $PbBr_2$ and 5 mL of ODE were taken in a 2-neck 50 mL reaction flask. The flask was heated at 120 °C under vacuum while stirring the solution mixture at 400 rpm. After 15 minutes of the temperature reaching 120 °C, 0.5 mL OA and 0.5 mL OAm were injected into the flask sequentially with plastic syringes (6 mL Luer Slip Plastic Syringe, Thermo Scientific, and Precision-glide Needle, BD). When the solution mixture in the flask turned a clear yellow color, the flask was heated to 180 °C under a N_2 environment. Then, preheated 0.4 mL Cs-oleate (maintained at 150 ^{o}C) was injected dropwise at a rate of 1-2 drop(s) per second in the flask. Finally, the flask was cooled down immediately to room temperature in an ice bath. As the solution cooled to room temperature, it turned a bright green color.

The $CsPbBr_3$ NCs were purified by taking 1.0 mL of crude solution and centrifuging at 10000 rpm for 5 minutes and discarding the colored supernatant. Then $CsPbBr_3$ NCs were dispersed in 300 μL hexane, and the solution was centrifuged at 10000 rpm for 5 minutes. Supernatant was collected and stored in a vial in air. Total volume of stock dispersion of $CsPbBr_3$ NCs was 1.8 mL.

Synthesis of $PbCl_2$ assisted anion exchanged $CsPbCl_3$ NCs

19.467 mg $PbCl_2$ along with 0.5 mL TOP was mixed with 2.5 mL ODE in a 50 mL 2-neck flask and kept under vacuum at 120 °C for more than 10 minutes while stirring at 400 rpm. OA and OAm (0.25 mL each) were injected at 120 °C under vacuum. For complete dissolution of $PbCl_2$, the temperature of the flask was raised to 170 °C for 10-15 minutes under a N_2 environment. After dissolution of $PbCl_2$, the temperature of the flask was lowered to 40 °C and $CsPbBr_3$ NCs (before adding, 155 μL of pure $CsPbBr_3$ NCs was diluted in 345 μL hexane) was injected in the dissolved $PbCl_2$ to initiate the anion exchange to form colloidal $CsPbCl_3$ NCs. Purification of this sample was also carried out in the same manner as that of colloidal $CsPbBr_3$ NCs. Total volume of colloidal dispersion of $CsPbCl_3$ was 1.2 mL.

Synthesis of DTS assisted anion exchanged $CsPbCl_3$ NCs

Differing volumes of DTS, as specified in the text, were added to the initially purified colloidal $CsPbBr_3$ NC suspension. For FTIR and Raman samples, the crude solution was centrifuged at 10000 rpm for 30 minutes, and the supernatant was collected. The $CsPbCl_3$ NCs in the pellet were dispersed in hexane again. For time-dependent PLQYs and lifetime measurements, DTS assisted anion exchanged NCs were used directly without further purification.

For solid films and XRD Samples, 250 μL of stock dispersion of $CsPbBr_3$ NCs was diluted to 2.5 mL with hexane. Then 1 mL of DTS and 0.5 mL of distilled water were added to the NCs, respectively. Then 1 mL of crude dispersion of $CsPbCl_3$ NCs was centrifuged at 10000 rpm for 30 minutes, and the supernatant was collected for preparing solid thin films. NCs in the pellet were re-dispersed in 1.2 mL of hexane and centrifuged again at 10000 rpm for 3 minutes, and the supernatant was collected and used for preparing XRD samples.

Stability Measurements

For $PbCl_2$ assisted anion exchanged NCs, 100 μL deionized water was directly added to 3 mL of colloidal $CsPbCl_3$ NCs (absorbance values of *ca.* 0.1 at 350 nm). After inverting the capped cuvette several times, PL emission spectra were collected. A similar procedure was followed for DTS assisted anion exchanged $CsPbCl_3$ NCs. For thin films, DTS assisted anion exchanged NCs were deposited on a glass substrate by drop casting. After the sample was dry, time dependent PL emission spectra were collected.

CHARACTERIZATION

Optical absorption spectra were collected using an Ocean Optics QE pro high-performance spectrometer with 80 millisecond integration time and 5 micron slit width. Fluorescence emission spectra were measured using a Lumina Fluorescence Spectrometer by Thermo Fisher Scientific with 20 millisecond integration time and 2.5 nm slit

width (PL data in SI Figure S11 were collected with a Horiba Scientific Fluoromax Plus-C Flouorimeter with 1.25 and 0.5 nm slits for SI Figures S11a and S11b, respectively). For collecting PL data, purified NC solutions were diluted in hexane to reach an optical absorbance of 0.05-0.1 at the excitation wavelength. PL emission spectra were collected by exciting the samples at 350 nm for colloidal $CsPbCl_3$ NCs and at 405 nm for colloidal $CsPbBr_3$ NCs. For PLQY measurements, the purified NC solutions were diluted in hexane to reach an optical absorbance of 0.05-0.1 at the excitation wavelength. The spectra were collected using a Horiba Scientific Fluoromax Plus-C Fluorimeter equipped with an integrating sphere by exciting the samples with a 350 nm excitation wavelength for $CsPbCl_3$ NCs and a 405 nm excitation wavelength for $CsPbBr_3$ NCs. Emission was scanned to include the Rayleigh scattering from the hexane solvent. Photoluminescence lifetimes were measured using a DeltaHub™ high throughput time correlated single photon counting (TCSPC) controller with an excitation wavelength of 393 nm generated by a pulsed NanoLED excitation source. Experimental PL lifetime results were fitted with exponential decay curves using Horiba Scientific Decay Analysis Software. FTIR data were obtained with a Thermo Scientific Nicolet IS50 FTIR Spectrometer equipped with a diamond ATR plate. A resolution of 4 cm^{-1} and 64 scans were used in each measurement. Purified NCs were drop cast on a glass slide and Raman spectra were obtained with a Thermo Scientific Raman Microscope DXR equipped with a 10x objective lens. Raman measurements were carried out with a laser power of 10 mW and an excitation wavelength of 532 nm. A resolution of 4 cm^{-1} and 64 scans were used in each measurement. TEM samples were prepared on lacey carbon films supported by 300 mesh copper and TEM images were obtained using a JEOL 2010F operated at 200 kV. The X-ray diffraction patterns (θ-2θ scans) were taken on a Bruker-AXS D8 DISCOVER diffractometer with Cu Kα radiation (λ = 1.5418 Å) operating at 40 kV and 40 mA. Samples for XRD measurements were prepared by drop casting perovskite NC dispersions on glass substrates and drying under vacuum.

CONFLICTS OF INTEREST

There are no conflicts to declare.

ACKNOWLEDGEMENTS

This material is based upon work supported by the U.S. Department of Energy, Office of Science, Office of Basic Energy Sciences and the EPSCoR program, under Award Number DE-SC0018208. The TCSPC instrument was purchased by the support from the University of Kentucky, Vice President of Research Equipment grant.

REFERENCES

1 B. A. Koscher, J. K. Swabeck, N. D. Bronstein and A. P. Alivisatos, *J. Am. Chem. Soc.*, 2017, **139**, 6566–6569.
2 A. Swarnkar, R. Chulliyil, V. K. Ravi, M. Irfanullah, A. Chowdhury and A. Nag, *Angew. Chemie*, 2015, **127**, 15644–15648.
3 S. Huang, Z. Li, L. Kong, N. Zhu, A. Shan and L. Li, *J. Am. Chem. Soc.*, 2016, **138**, 5749–5752.
4 L. Protesescu, S. Yakunin, M. I. Bodnarchuk, F. Krieg, R. Caputo, C. H. Hendon, R. X. Yang, A. Walsh and M. V. Kovalenko, *Nano Lett.*, 2015, **15**, 3692–3696.
5 M. Liu, M. B. Johnston and H. J. Snaith, *Nature*, 2013, **501**, 395–398.
6 N. J. Jeon, J. H. Noh, W. S. Yang, Y. C. Kim, S. Ryu, J. Seo and S. Il Seok, *Nature*, 2015, **517**, 476–480.
7 M. Kulbak, S. Gupta, N. Kedem, I. Levine, T. Bendikov, G. Hodes and D. Cahen, *J. Phys. Chem. Lett.*, 2016, **7**, 167–172.
8 Q. A. Akkerman, M. Gandini, F. Di Stasio, P. Rastogi, F. Palazon, G. Bertoni, J. M. Ball, M. Prato and A. Petrozza, *Nat. Energy*, 2016, **1**, 1–7.
9 J. Wang, N. Wang, Y. Jin, J. Si, Z. K. Tan, H. Du, L. Cheng, X. Dai, S. Bai, H. He, Z. Ye, M. L. Lai, R. H. Friend and W. Huang, *Adv. Mater.*, 2015, **27**, 2311–2316.
10 X. Zhang, H. Lin, H. Huang, C. Reckmeier, Y. Zhang, W. C. H. Choy and A. L. Rogach, *Nano Lett.*, 2016, **16**, 1415–1420.
11 J. Song, J. Li, X. Li, L. Xu, Y. Dong and H. Zeng, *Adv. Mater.*, 2015, **27**, 7162–7167.
12 L. Zhang, X. Yang, Q. Jiang, P. Wang, Z. Yin, X. Zhang, H. Tan, Y. M. Yang, M. Wei, B. R. Sutherland, E. H. Sargent and J. You, *Nat. Commun.*, 2017, **8**, 1–8.
13 S. Yakunin, L. Protesescu, F. Krieg, M. I. Bodnarchuk, G. Nedelcu, M. Humer, G. De Luca, M. Fiebig, W. Heiss and M. V. Kovalenko, *Nat. Commun.*, 2015, **6**, 1–8.
14 Y. Xu, Q. Chen, C. Zhang, R. Wang, H. Wu, X. Zhang, G. Xing, W. W. Yu, X. Wang, Y. Zhang and M. Xiao, *J. Am. Chem. Soc.*, 2016, **138**, 3761–3768.
15 Y. Fu, H. Zhu, C. C. Stoumpos, Q. Ding, J. Wang, M. G. Kanatzidis, X. Zhu and S. Jin, *ACS Nano*, 2016, **10**, 7963–7972.
16 F. Deschler, M. Price, S. Pathak, L. E. Klintberg, D. D. Jarausch, R. Higler, S. Hüttner, T. Leijtens, S. D. Stranks, H. J. Snaith, M. Atatüre, R. T. Phillips and R. H. Friend, *J. Phys. Chem. Lett.*, 2014, **5**, 1421–1426.
17 L. Dou, Y. M. Yang, J. You, Z. Hong, W. H. Chang, G. Li and Y. Yang, *Nat. Commun.*, 2014, **5**, 1–6.
18 P. Ramasamy, D.-H. Lim, B. Kim, S.-H. Lee, M.-S. Lee and J.-S. Lee, *Chem. Commun.*, 2016, **52**, 2067–2070.
19 B. R. Sutherland, A. K. Johnston, A. H. Ip, J. Xu, V. Adinolfi, P. Kanjanaboos and E. H. Sargent, *ACS Photonics*, 2015, **2**, 1117–1123.
20 R. Dong, Y. Fang, J. Chae, J. Dai, Z. Xiao, Q. Dong, Y. Yuan, A. Centrone, X. C. Zeng and J. Huang, *Adv. Mater.*, 2015, **27**, 1912–1918.
21 G. Nedelcu, L. Protesescu, S. Yakunin, M. I. Bodnarchuk, M. J. Grotevent and M. V. Kovalenko, *Nano Lett.*, 2015, **15**, 5635–5640.
22 D. Aldakov, A. Lefrançois and P. Reiss, *J. Mater. Chem. C*, 2013, **1**, 3756.
23 H. Y. Ueng and H. L. Hwang, *J. Phys. Chem. Solids*, 1989, **50**, 1297–1305.
24 L. De Trizio, M. Prato, A. Genovese, A. Casu, M. Povia, R. Simonutti, M. J. P. Alcocer, C. D'Andrea, F. Tassone and L. Manna, *Chem. Mater.*, 2012, **24**, 2400–2406.

25 W. Zhang and X. Zhong, *Inorg. Chem.*, 2011, **50**, 4065–4072.
26 L. Protesescu, S. Yakunin, M. I. Bodnarchuk, F. Bertolotti, N. Masciocchi, A. Guagliardi and M. V. Kovalenko, *J. Am. Chem. Soc.*, 2016, **138**, 14202–14205.
27 H. Huang, M. I. Bodnarchuk, S. V. Kershaw, M. V. Kovalenko and A. L. Rogach, *ACS Energy Lett.*, 2017, **2**, 2071–2083.
28 J. De Roo, M. Ibáñez, P. Geiregat, G. Nedelcu, W. Walravens, J. Maes, J. C. Martins, I. Van Driessche, M. V. Kovalenko and Z. Hens, *ACS Nano*, 2016, **10**, 2071–2081.
29 A. A. A. Pan, B. He, X. Fan, Z. Liu, J. J. Urban, A. P. Alivisatos, L. He, Y. Liu and A. Paul, *ACS Nano*, 2016, **10**, 7943–7954.
30 G. Li, J. Y. L. Ho, M. Wong and H. S. Kwok, *J. Phys. Chem. C*, 2015, **119**, 26883–26888.
31 G. Rainoì, G. Nedelcu, L. Protesescu, M. I. Bodnarchuk, M. V. Kovalenko, R. F. Mahrt and T. Stöferle, *ACS Nano*, 2016, **10**, 2485–2490.
32 J. Mizusaki, K. Arai and K. Fueki, *Solid State Ionics*, 1983, **11**, 203–211.
33 J. M. Azpiroz, E. Mosconi, J. Bisquert and F. De Angelis, *Energy Environ. Sci.*, 2015, **8**, 2118–2127.
34 C. Eames, J. M. Frost, P. R. F. Barnes, B. C. O'Regan, A. Walsh and M. S. Islam, *Nat. Commun.*, 2015, **6**, 2–9.
35 M. Li, X. Zhang, S. Lu and P. Yang, *RSC Adv.*, 2016, **6**, 103382–103389.
36 Q. A. Akkerman, V. D'Innocenzo, S. Accornero, A. Scarpellini, A. Petrozza, M. Prato and L. Manna, *J. Am. Chem. Soc.*, 2015, **137**, 10276–10281.
37 T. Zhang, G. Li, Y. Chang, X. Wang, B. Zhang, H. Mou and Y. Jiang, *CrystEngComm*, 2017, **19**, 1165–1171.
38 C. Guhrenz, A. Benad, C. Ziegler, D. Haubold, N. Gaponik and A. Eychmüller, *Chem. Mater.*, 2016, **28**, 9033–9040.
39 D. Parobek, Y. Dong, T. Qiao, D. Rossi and D. H. Son, *J. Am. Chem. Soc.*, 2017, **139**, 4358–4361.
40 A. Pan, B. He, X. Fan, Z. Liu, J. J. Urban, A. P. Alivisatos, L. He and Y. Liu, *ACS Nano*, 2016, **10**, 7943–7954.
41 L. Ruan, W. Shen, A. Wang, Q. Zhou, H. Zhang and Z. Deng, *Nanoscale*, 2017, **9**, 7252–7259.
42 M. Shirayama, M. Kato, T. Miyadera, T. Sugita, T. Fujiseki, S. Hara, H. Kadowaki, D. Murata, M. Chikamatsu and H. Fujiwara, *J. Appl. Phys.*, 2016, **119**, 115501.
43 J. Yang, B. D. Siempelkamp, D. Liu and T. L. Kelly, *ACS Nano*, 2015, **9**, 1955–1963.
44 L. Zhang, M.-G. Ju and W. Liang, *Phys. Chem. Chem. Phys.*, 2016, **18**, 23174–23183.
45 G. Niu, X. Guo and L. Wang, *J. Mater. Chem. A*, 2015, **3**, 8970–8980.
46 S. Wang, Y. Jiang, E. J. Juarez-Perez, L. K. Ono and Y. Qi, *Nat. Energy*, 2017, **2**, 2009–2014.
47 B. Luo, Y. C. Pu, S. A. Lindley, Y. Yang, L. Lu, Y. Li, X. Li and J. Z. Zhang, *Angew. Chemie - Int. Ed.*, 2016, **55**, 8864–8868.
48 M. Meyns, M. Perálvarez, A. Heuer-Jungemann, W. Hertog, M. Ibáñez, R. Nafria, A. Genç, J. Arbiol, M. V. Kovalenko, J. Carreras, A. Cabot and A. G. Kanaras, *ACS Appl. Mater. Interfaces*, 2016, **8**, 19579–19586.
49 H. Huang, B. Chen, Z. Wang, T. F. Hung, A. S. Susha, H. Zhong and A. L. Rogach, *Chem. Sci.*, 2016, **7**, 5699–5703.
50 C. A. Cattley, A. Stavrinadis, R. Beal, J. Moghal, A. G. Cook, P. S. Grant, J. M. Smith, H. Assender and A. A. R. Watt, *Chem. Commun.*, 2010, **46**, 2802.
51 L. Wu, Q. Zhong, D. Yang, M. Chen, H. Hu, Q. Pan, H. Liu, M. Cao, Y. Xu, B. Sun and Q. Zhang, *Langmuir*, 2017, **33**, 12689–12696.
52 S. Gonzalez-Carrero, L. Francés-Soriano, M. González-Béjar, S. Agouram, R. E. Galian and J. Pérez-Prieto, *Small*, 2016, 5245–5250.
53 F. Krieg, S. T. Ochsenbein, S. Yakunin, S. Ten Brinck, P. Aellen, A. Süess, B. Clerc, D. Guggisberg, O. Nazarenko, Y. Shynkarenko, S. Kumar, C. J. Shih, I. Infante and M. V. Kovalenko, *ACS Energy Lett.*, 2018, **3**, 641–646.
54 J. Wang, X. Xiang, X. Yao, W. J. Xiao, J. Lin and W. S. Li, *Org. Electron. physics, Mater. Appl.*, 2016, **39**, 1–9.
55 R. P. Pohanish, *Sittig's Handbook of Toxic and Hazardous Chemicals and Carcinogens*, Elsevier Inc., 225 Wyman Street, Waltham, MA 02451, USA, 6th edn., 2012.
56 W. Cao, P. Liu, W. Chen, W. Wang, B. Xu, D. Wu, J. Hao, W. Cao, F. Fang, Y. Li, Y. Zeng, R. Pan, S. Chen, X. W. Sun and K. Wang, *Chem. Mater.*, 2017, **29**, 5168–5173.
57 Y. Kim, E. Yassitepe, O. Voznyy, R. Comin, G. Walters, X. Gong, P. Kanjanaboos, A. F. Nogueira and E. H. Sargent, *ACS Appl. Mater. Interfaces*, 2015, **7**, 25007–25013.
58 M. Koolyk, D. Amgar, S. Aharon and L. Etgar, *Nanoscale*, 2016, **8**, 6403–6409.
59 S. Wei, Y. Yang, X. Kang, L. Wang, L. Huang and D. Pan, *Chem. Commun.*, 2016, **52**, 7265–7268.
60 S. Seth and A. Samanta, *Sci. Rep.*, 2016, **6**, 1–7.
61 D. Rossi, D. Parobek, Y. Dong and D. H. Son, *J. Phys. Chem. C*, 2017, **121**, 17143–17149.
62 S. Das Adhikari, S. K. Dutta, A. Dutta, A. K. Guria and N. Pradhan, *Angew. Chemie - Int. Ed.*, 2017, **56**, 8746–8750.
63 D. Parobek, B. J. Roman, Y. Dong, H. Jin, E. Lee, M. Sheldon and D. H. Son, *Nano Lett.*, 2016, **16**, 7376–7380.
64 F. Hu, H. Zhang, C. Sun, C. Yin, B. Lv, C. Zhang, W. W. Yu, X. Wang, Y. Zhang and M. Xiao, *ACS Nano*, 2015, **9**, 12410–12416.
65 X. Li, Y. Wu, S. Zhang, B. Cai, Y. Gu, J. Song and H. Zeng, *Adv. Funct. Mater.*, 2016, **26**, 2435–2445.
66 Q. Han, W. Wu, W. Liu and Y. Yang, *RSC Adv.*, 2017, **7**, 35757–35764.
67 Y. Wang, M. Zhi and Y. Chan, *J. Phys. Chem. C*, 2017, **121**, 28498–28505.
68 B. Guo, S. W. Tay, Z. Liu and L. Hong, *Polymers*, 2012, **4**, 1499–1516.
69 S. Gardelis, A. G. Nassiopoulou, M. Mahdouani, R. Bourguiga and S. Jaziri, *Phys. E Low-Dimensional Syst. Nanostructures*, 2009, **41**, 986–989.
70 D. Rajput, L. Costa, A. Terekhov, K. Lansford and W. Hofmeister, *Nanotechnology*, 2012, **23**, 105304.
71 E. Moyers-Montoya, P. García-Casillas, C. Vargas-Requena, R. Escobedo-González, S. A. Martel-Estrada and C. A. Martínez-Pérez, *Polymers*, 2016, **8**, 1–17.
72 J. M. Luther, M. Law, Q. Song, C. L. Perkins, M. C. Beard and A. J. Nozik, *ACS Nano*, 2008, **2**, 271–280.
73 A. Torreggiani and A. Tinti, *Metallomics*, 2010, **2**, 246.

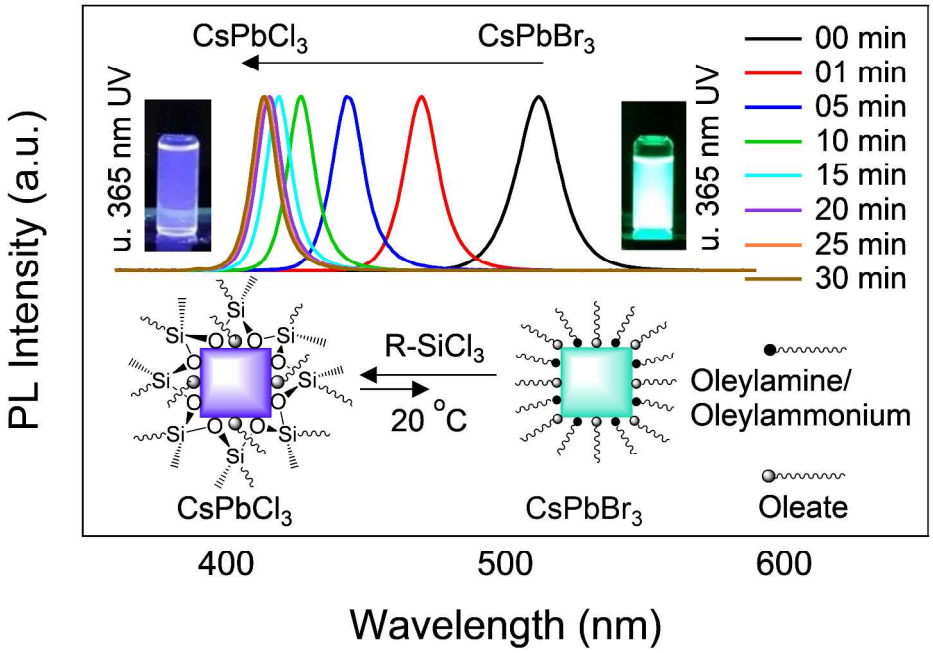

645x436mm (192 x 192 DPI)